

Temperature-induced Hollow Hierarchical NiCo₂O₄ Microspheres for High Performance Pseudocapacitors

Junbo Qin, Xinyi Chi, Junjie You*, Chuanqing Du and Siqing Cheng

Innovation Centre for Nanomaterials in Energy and Environment (ICNEE), School of Chemical and Environmental Engineering, Wuhan Polytechnic University, Hubei 430023, P. R. China

*E-mail: icnee@whpu.edu.cn

Received: 17 November 2021 / Accepted: 2 January 2022 / Published: 2 February 2022

Spinel nickel cobaltite (NiCo₂O₄) has been proved to be one of the most promising electrode materials for high performance supercapacitors due to its high theoretic specific capacitance, excellent electronic conductivity and good environmental benignity. In this work, the unique NiCo₂O₄ structure was fabricated hydrothermally via the induction of the reaction temperature and investigated electrochemically as supercapacitor electrode material. The resultant NiCo₂O₄ electrode with hollow hierarchical microspherical structure as supercapacitor displays excellent capacitive characteristic with higher specific capacitance, better cycling stability and rate capability compared to those with various morphologies, revealing the morphology dependence of the capacitive properties of NiCo₂O₄ electrode owing to the discrepant electronic conductivity and ion diffusion behavior. Thus, the temperature-induced changes in morphology are potential in the large-scale fabrication of NiCo₂O₄ electrode materials as supercapacitors.

Keywords: NiCo₂O₄, Electrode materials; Pseudocapacitors; Electrochemical performance.

1. INTRODUCTION

To address the gradual exhaustion of traditional non-renewable fossil fuels and the resultant severe environmental pollution issues, the ever-increasing demand to develop the new energy conversion and storage technologies, such as fuel cells, supercapacitors and rechargeable batteries as electrochemical energy storage devices for hybrid electric vehicles (HEVs), electric vehicles (EVs), plug-in hybrid electric vehicles (PHEVs), and smart grids have been highly focused. Thereinto, supercapacitors, also known as electrochemical capacitors, have aroused great interesting as one of the most promising candidates of clean energy storage devices owing to their inherent remarkable advantages over other conventional energy storage technologies, such as outstanding power density,

long lifespan, rapid charge/discharge capability, wide operation temperature range and improved safety.[1-4] However, the relatively low energy density greatly restricted their practical applications to certain extent as a primary power source in many important fields. Therefore, great efforts have made to improve their energy density without sacrificing their cycle lifespan and power density by designing the novel electrode materials with high capacity and tailored architectures.[5-8]

To date, diverse materials, including carbon-based materials, conducting polymers and transition metal oxides, have been widely investigated as the electrodes for supercapacitors, among which electric double-layer capacitor (EDLC) electrode materials and pseudocapacitive electrode materials are distinguished according to the underlying energy storage mechanism.[3, 5, 9, 10] Comparatively, diverse transition metal oxides, such as NiO, RuO₂, Co₃O₄, ZnO, V₂O₅, Fe₂O₃ and MnO₂ etc. have attracted more and more attention as pseudocapacitance electrode materials due to their fast multielectron Faradaic redox reaction resulting in a high specific capacitance.[11-14] Nevertheless, because of the poor intrinsic electrical conductivity with band gaps of ca. 4 eV, these transition metal oxides cannot demonstrate their outstanding electrochemical performance, especially the rate capability, unless they are modified by some good conductive materials.[15-17] Therefore, it is vital to devise some alternative electrode materials for pseudocapacitors with better electrical conductivity.

To effectively overcome the poor electrical conductivity of transition metal oxides as pseudocapacitor electrode materials, some binary composites of transition metal oxides are of particular interest due to their plentiful structure defects that are in favor of fast redox reactions.[17-20] Among them, spinel nickel cobaltite (NiCo₂O₄) with similar crystal structure of Co₃O₄ using Ni atoms to replace partially Co atoms exhibits a promising electrochemical performance due to its much better electronic conductivity compared with single nickel oxides or cobalt oxides, high theoretical capacity and environmental benignity.[21-24] Various structures and morphologies of NiCo₂O₄ as pseudocapacitance electrode materials have been investigated to demonstrate superior capacitive properties, whereas the rate capabilities and cycling stability of the electrode materials usually are not satisfactory due to the pronounced volumetric expansion of the electrode materials during charge/discharge processes.[25-27] Thus, the hollow morphology of NiCo₂O₄ electrode materials has been engineered elaborately to provide additional free space to accommodate the volume changes during the electrochemical processes by many methods such as the electro-deposition process, the sol-gel method and microwave technique etc.[28-30] However, these methods used are not suitable to large-scale production of NiCo₂O₄ for the practical applications due to relatively complicated procedures, high cost and time-consuming. Therefore, the rational preparation of the promising NiCo₂O₄-based electrode materials with desirable structure and morphology still remains a challenge.

In this paper, the morphology of NiCo₂O₄ electrode materials were tuned hydrothermally by the evolution of reaction temperature, and the capacitive electrochemical performance of the resultant NiCo₂O₄ electrode materials is variable remarkably, implying the hydrothermal reaction temperature dependence of the morphology of NiCo₂O₄ electrode materials and thus the variation in the capacitive electrochemical properties.

2. EXPERIMENTAL SECTION

2.1 Materials

All Chemicals used were of analytical grade and used as received without further purification unless otherwise stated. Thereinto, nickel nitrate hexahydrate (99.6%, $\text{Ni}(\text{NO}_3)_2 \cdot 6\text{H}_2\text{O}$), cobalt nitrate hexahydrate (99.5%, $\text{Co}(\text{NO}_3)_2 \cdot 6\text{H}_2\text{O}$) were purchased from Tianjin Damao Chemical Reagent Co. Ltd., Urea (99.8%, $\text{CH}_4\text{N}_2\text{O}$) and potassium hydroxide (99.8%, KOH) were supplied by Sinopharm. Chemical Reagent Co. Ltd. The de-ionized (DI) water was homemade in the laboratory.

2.2 Syntheses of NiCo_2O_4 materials

NiCo_2O_4 materials were prepared via a hydrothermal method followed by an annealing process. Typically, 2 mmol of $\text{Ni}(\text{NO}_3)_2 \cdot 6\text{H}_2\text{O}$, 4 mmol of $\text{Co}(\text{NO}_3)_2 \cdot 6\text{H}_2\text{O}$ and 30 mmol of urea were dissolved thoroughly in 100 mL beaker containing 60 g of water by stirring magnetically. The as-obtained NiCo_2O_4 precursor was introduced in a sealed Teflon-lined stainless-steel autoclave and heated in an oven at different temperature for 12 hours. After cooled naturally to room temperature, the solution was subjected to separate by the centrifugation and washed several times with DI water and absolute ethanol under ultrasonic conditions. The resultant precipitation was dried in a vacuum drying oven at 60 °C for 12 hours to obtain the violet solids. Thereafter, the as-synthesized violet solids were calcined in a muffle furnace at 350 °C for 4 hours to yield the desired black products. The resultant NiCo_2O_4 materials at the reaction temperature of 120 °C, 130 °C, 140 °C, 150 °C were remarked thereafter by NCO-1, NCO-2, NCO-3, NCO-4, respectively.

2.3 Characterization of NiCo_2O_4 Materials

An X-ray powder diffractometer (XRD, D/Max-2400, Digaku, Japan) using a Cu $K\alpha$ source ($\lambda=0.1541$ nm) with the tube voltage of 45 kV was employed to identify the structure of samples with the diffraction angle (2θ) range from 20° to 80° at a scan rate of 4° min^{-1} . The morphologies of the as-obtained samples were observed by scanning electron microscopy (SEM, JSM-6701, JOEL) at different magnification.

2.4 Electrochemical measurements

All electrochemical performances of the as-prepared electrodes were performed in 2 M KOH aqueous solution on a CHI-660B electrochemical workstation (Chenghua, Shanghai, China) in an open three-electrode cell configuration at room temperature. The typical working electrode was prepared using the following procedures: a uniform slurry was obtained by mixing the as-synthesized active NiCo_2O_4 materials, the binder polyvinylidene fluoride (PVDF) and the conducting agent carbon black BP-200 with the weight ratio of 8:1:1 in the solvent N-methyl pyrrolidone (NMP), and followed by coating the slurry on foamed nickel (1×1 cm^2) and then vacuum drying at 80 °C to form the working

electrode with the active materials mass loaded of ~ 5 mg. A platinum sheet and a Hg/HgO (SCE) were used as the counter electrode and the reference electrode, respectively. The Galvanostatic charge/discharge (GCD) curves were measured with the potential window from 0 to 0.7 V (versus SCE) at the various constant current density ranging from 1 to 10 A g⁻¹. The cyclic voltammetry (CV) was carried out with the same potential window as GCD tests at different sweep rates varying from 2 to 50 mV s⁻¹. The electrochemical impedance spectroscopy (EIS) plots were recorded in an alternating current frequency ranging from 100 kHz to 0.01 Hz at open circuit potential of 0.25 V with a perturbation signal of 5 mV. The specific capacitances of the electrodes were calculated from the corresponding discharge curves by the following formula[31-33]:

$$C = \frac{I\Delta t}{m\Delta V} \quad (1)$$

where C is the specific capacitance in F g⁻¹, I is the constant discharging current in A, Δt is the discharge time in s, ΔV is the window potential during the discharge process after the internal resistance (IR) drop (V), and m is the mass of the active electrode material in g.

3. RESULTS AND DISCUSSION

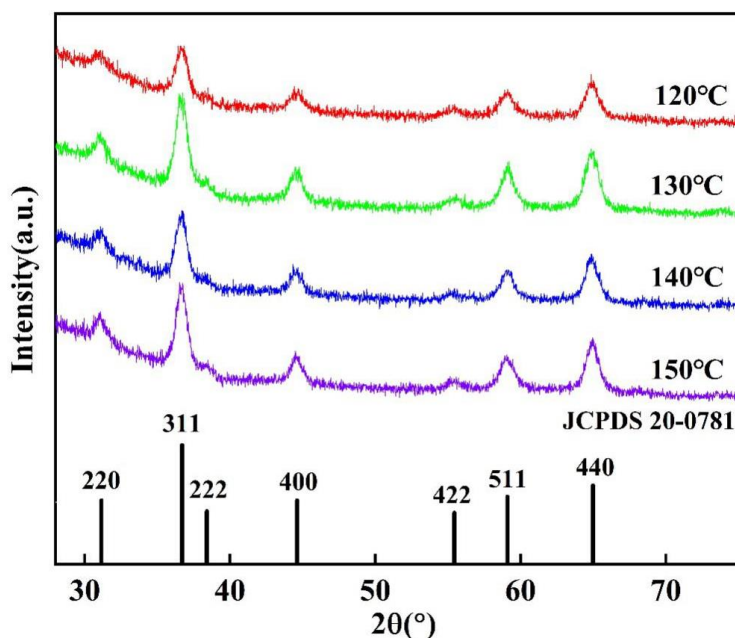


Figure 1. XRD patterns of the as-synthesized NiCo₂O₄ materials at various temperature

To identify the crystallinity, phase and purity of the as-obtained NiCo₂O₄ samples, X-ray powder diffraction (XRD) was exploited to detect the phase compositions, as shown in Fig. 1. From Fig. 1, it could be seen that the as-obtained NiCo₂O₄ materials demonstrate several well-defined diffraction peaks at 2θ values of 31.15°, 36.6°, 38.4°, 44.62°, 55.44°, 59.09° and 64.98°, which can be well indexed as the (220), (311), (222), (400), (422), (511) and (440) plane reflections of the standard spinel NiCo₂O₄ crystalline structure (JCPDS:20-02781)[34, 35], respectively, without any excrescent peaks from other crystallized phases to be detected, manifesting the pure composition of the as-synthesized spinel NiCo₂O₄ crystalline structure (space group *Fd3m*) with nickel located at the octahedral interstices and

cobalt occupied among the octahedral and tetrahedral interstices to offer a three dimensional network of tunnels favorable for ion diffusion. Apparently, there seems no difference for the XRD patterns of the as-synthesized NiCo_2O_4 materials at various reaction temperature. However, the relative broad peaks in XRD patterns in Fig.1 demonstrate the small crystallite size and the relative low crystallinity, and the discrepancy in the peak breadth is obvious at different reaction temperature, which is expected to have a diverse electrochemical activity for different NiCo_2O_4 materials at various reaction temperature. According to the Debye-Scherrer formula[36], the average crystallite size of the prepared NiCo_2O_4 could be calculated approximately to be about 8.6 nm, 12.4 nm, 15.8 nm and 18.7 nm for NCO-1, NCO-2, NCO-3, NCO-4, respectively, by analyzing the marked (311) plane reflection peak in XRD pattern. Fig. 2 presents the different morphology of the synthesized NiCo_2O_4 at various reaction temperature. It is obvious that NiCo_2O_4 powders are some well-knit irregular spherical particles which consists of the agglomerated nanoparticles at relative low reaction temperature (Fig. 2a), as predicted in XRD patterns. When increasing the synthesized temperature to 150 °C, the loose urchin-like hollow NiCo_2O_4 microspheres are resulted from the temperature dependence of the aggregation of needle-like NiCo_2O_4 nanoparticles, as shown in the insets of Fig. 1 for the large magnification of SEM images, which would be responsible for the improved electrochemical performance, suggesting the tunability of the morphology by the reaction temperature on the favorable structure for the electrochemical activity.

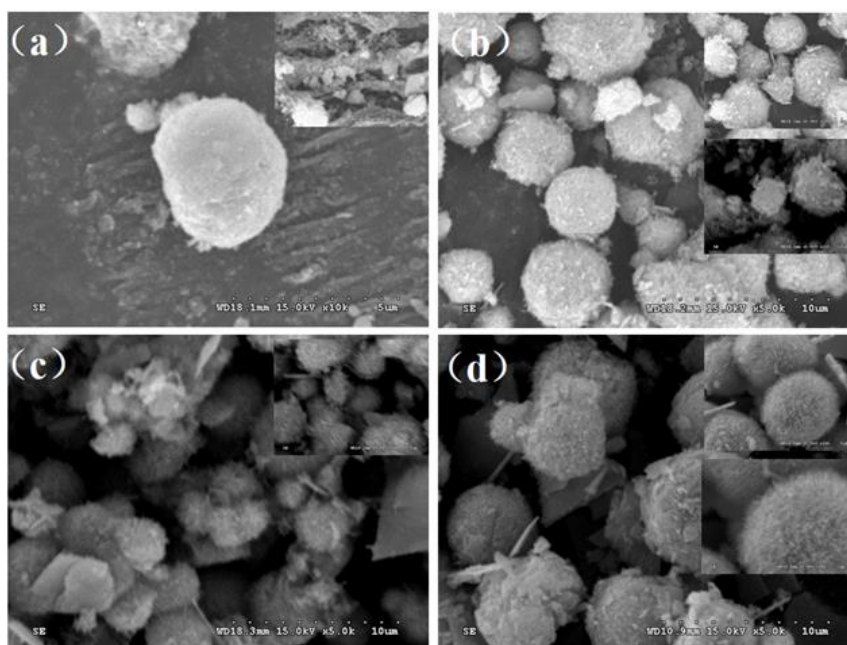


Figure 2. SEM images of the as-prepared NiCo_2O_4 materials at different temperature. (a) NCO-1, (b) NCO-2, (c) NCO-3, (d) NCO-4. The inset shows the SEM images at large magnification.

The three-electrode cell configuration in 2 M KOH aqueous solution was assembled to investigate the electrochemical properties of the as-obtained NiCo_2O_4 materials as the electrode for supercapacitor using cyclic voltammetry (CV), galvanostatic charge/discharge (GCD) and electrochemical impedance spectra (EIS). CV measurements are performed at the different sweep rates in the potential window ranging from -0.2 to 0.8 V (versus Hg/HgO), as shown typically in Fig. 3(a) for

the CV curves of NCO-4 electrode. Evidently, all CV curves of the investigated four NiCo₂O₄ electrodes show two broadened redox peaks due to the overlap of similar electrochemical redox potentials of Ni²⁺/Ni³⁺ and Co³⁺/Co⁴⁺ in the alkaline electrolyte[37, 38], implying the capacitive characteristic governed by the Faradaic reaction, i.e. pseudocapacitive behavior, compared with the rectangular CV curves of the traditional electrical double layer capacitors (EDLCs). Interestingly, with increasing the sweep rate from 2 to 50 mV s⁻¹, the anodic and cathodic peaks shift toward more positive and more negative potentials, respectively, and the redox current increases, which is mainly correlated to the polarization and the internal low resistance of the electrode, suggesting the rapid electronic transport rate in the electrode and good rate capability of the as-obtained NiCo₂O₄ electrodes.[39] To further elucidate the electrochemical capacitance discrepancy of the four synthesized electrodes, we are able to use the voltammetric scan rate dependence of peak current to determine quantitatively the capacitive contribution to the current response, as presented in the eqn.(2).[40, 41]

$$i=av^b \quad (2)$$

where a and b are the adjustable values, v is the sweep rate and i is the peak current of CV curves. Herein, the b value indicates the energy storage procedure. Generally, the capacitance is attributed to the ion adsorption on the electrode surface as the b value equals to be about 1 while the capacitance is ascribed to the ion diffusion due to the Faradaic reaction when the b value is about 0.5. As shown in Fig 3(b) for the plots of $\log(i)$ as a function of $\log(v)$, the b values of the four investigated electrodes are 0.7378, 0.7384, 0.7385 and 0.7457, respectively. This shows that the investigated NiCo₂O₄ materials as electrodes for supercapacitors exhibit the tendency of the synergy of both ion adsorption and both ion diffusion capacitance distribution, especially the NCO-4 electrode displays the almost equal contribution from ion adsorption and ion diffusion capacitance, indicating further the pseudocapacitive characteristic and thereby the structure dependence of the electrochemical performance for pseudocapacitor.

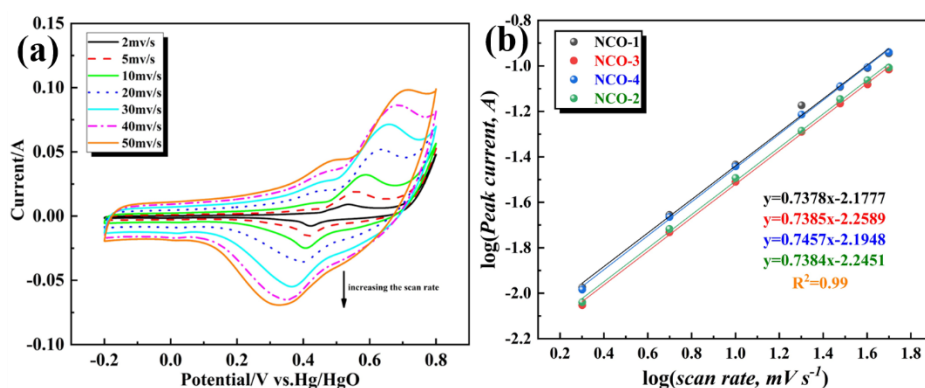


Figure 3. (a) Typical CV curves of NCO-4 electrode at various scan rate, (b) Plots of $\log(\text{anode peak current})$ as a function of $\log(\text{scan rate})$ at a specific anode peak current for the investigated four electrodes NCO-1, NCO-2, NCO-3 and NCO-4.

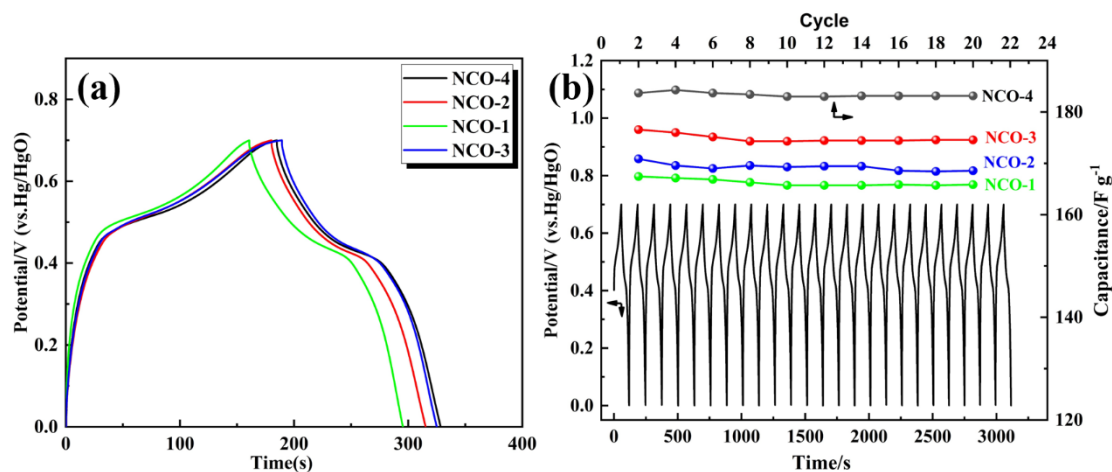


Figure 4. (a) GCD curves for the four investigated electrodes at the current density of 1 A g^{-1} , (b) Cycling stability for the four investigated electrodes as supercapacitors at the current density of 1 A g^{-1} and GCD curves at the continuous cycles for the NCO-4 electrode.

The GCD tests were performed with the potential window between 0 and 0.7 V versus SCE at the current density ranging from 1 to 10 A g^{-1} , the corresponding specific capacitances are calculated by eqn.(1). As has been seen from Fig. 4(a) that the GCD curves of the as-prepared NiCo_2O_4 electrodes at the current density of 1 A g^{-1} exhibit the pure faradaic capacitive characteristics and could be separated into two obvious regions with a sharp linear region between 0-0.4 V responsible for the capacitance due to the EDLCs and a long voltage plateaus between 0.4-0.7 V responsible for the capacitance due to the interfacial faradaic redox reaction, illustrating undoubtedly the typical pseudocapacitive behavior of the investigated NiCo_2O_4 electrodes, which is also in accordance with the aforementioned CV results. The calculated specific capacitances at the current density of 1 A g^{-1} are 183.71, 176.57, 170.86, 167.43 F g^{-1} , respectively for NCO-4, NCO-3, NCO-2, NCO-1 electrodes, demonstrating the highest discharge specific capacitance due to the longest discharge time for NCO-4 electrode with integrated hollow hierarchical structure induced by the temperature. Further, Fig.4b presents the cycle stabilities of the synthesized NiCo_2O_4 electrodes at the current density at 1 A g^{-1} using the repeated GCD cycles. From Fig.6, it could be seen that the stability of the specific capacitance varies remarkably for the synthesized NiCo_2O_4 electrodes, the NCO-4 electrode as supercapacitor exhibits an overwhelming stability with only minor fluctuation with only 1% decay of the initial capacitance after 20 cycles, implying strongly the good discharge cycling stability and long-term cycle life for the typical unique NiCo_2O_4 electrode. Additionally, the rate capability of a supercapacitor is of importance to optimize the capacitive materials. As presented in Fig. 5a for the specific capacitances at different current densities, it is obvious that the specific capacitance decreases gradually with increasing the current density from 1 to 10 A g^{-1} and markedly for the NCO-4 electrode, the specific capacitance at the current density of 10 A g^{-1} still remains at 149.81 F g^{-1} , showing the 81.5% retention of the specific capacitance of 183.71 F g^{-1} at the initial current density of 1 A g^{-1} , which is evident of better rate capability compared to other NCO-1, NCO-2 and NCO-3 electrodes. This might be ascribed to the reduction in the diffusion resistance of electrolyte and thus to the fast ion transport during the charge/discharge process at high current densities due to the

hollow hierarchical NiCo₂O₄ structure, which would be further corroborated by the AC impedance spectra.

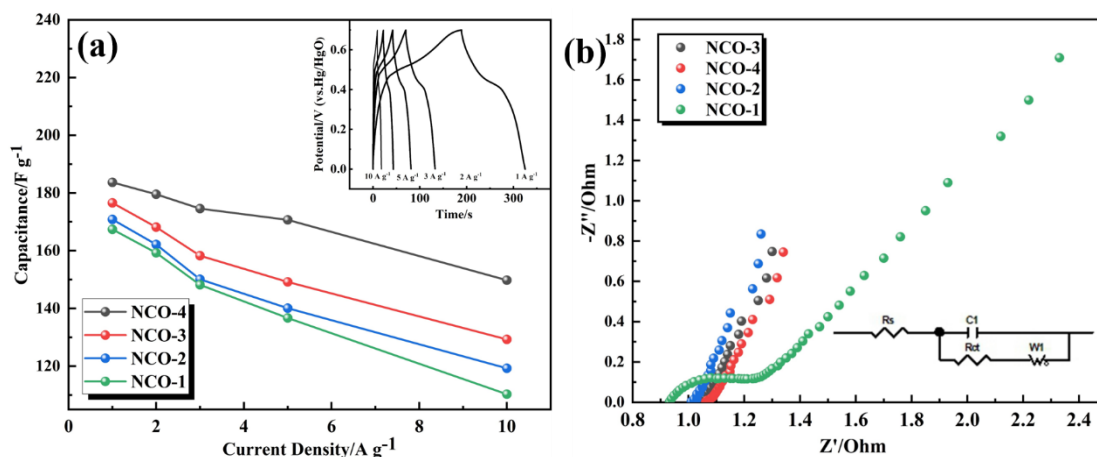


Figure 5. (a) Specific capacitance for the four investigated electrodes as supercapacitor as a function of the discharge current density. Inset: GCD curves for the NCO-4 electrode as supercapacitor at different discharge current densities. (b) Nyquist plots of the four investigated electrodes as supercapacitors at open circuit voltage of 0.25 V with a perturbation signal of 5 mV in an AC frequency ranging from 100 kHz to 0.01 Hz. Inset: the electrical equivalent circuit used for fitting impedance spectra.

Electrochemical impedance spectroscopy (EIS) tests were carried out within the frequency from 100 kHz to 0.01 Hz and the resulting Nyquist plots are presented in Fig. 5b, whose inset is the proposed equivalent circuit for the analyzed impedance data, including the electrolyte resistance (R_s) referring to be as the intersecting point with the real axis in the higher frequency, electric double layer capacitance (C_1), Faradaic charge transfer resistance (R_{ct}) at the electrode-electrolyte interface relating to the diameter of the semicircle in the high and intermediate frequency, a Warburg element (Z_w) corresponding to the vertical line in the low frequency region.[42-44] From Fig.5b, it is shown that the low R_s and R_{wt} in the all Nyquist plots indicates a good electron transfer property of NiCo₂O₄ electrode, which is favorable to ameliorate the electrochemical performance of the investigated materials. Comparing the Warburg impedance of different NiCo₂O₄ electrodes, it is shown that the straight line for the NCO-4 electrode is closer to the imaginary impedance axis in the Nyquist plots, illustrating the more ideal capacitive behavior and faster ion diffusion ability on the electrode surface for the NCO-4, which is responsible for the aforementioned better electrochemical performance.

4. CONCLUSION

In summary, the capacitive NiCo₂O₄ electrode materials were fabricated successfully to be the hollow hierarchical microsphere structure by the induction of the hydrothermal reaction temperature,

illustrating the reaction temperature dependence of the morphology and structure of the NiCo₂O₄ electrode materials. The comparative investigations on the electrochemical performances of the as-prepared NiCo₂O₄ materials by hydrothermal method at different temperatures show that the structure and morphology of the investigated NiCo₂O₄ materials exhibit great influence on the capacitive characteristics including the discharge specific capacitance, cycling stability and rate capability, among which the hollow hierarchical NiCo₂O₄ microspheres as supercapacitor electrode materials are more beneficial for the capacitive properties due to its better electronic conductivity, large specific surface area and more favorable ion diffusion, which has been corroborated further by the electrochemical impedance spectra. Therefore, the proposed fabrication of temperature-induced hollow hierarchical NiCo₂O₄ microspheres are prospective in the industrial implementation of large-scale production of NiCo₂O₄ electrode materials as supercapacitors.

ACKNOWLEDGEMENTS

The work was supported by the Scientific Research Project for College Students of WHPU (no. xsky2021037) and by Research and Innovation Initiatives of WHPU (no.2020Y06).

References

1. A. Afif, S. M. H. Rahman, A. Tasfiah Azad, J. Zaini, M. A. Islan and A. K. Azad. *J. Energy Storage*, 25 (2019) 100852.
2. K. K. Patel, T. Singhal, V. Pandey, T. P. Sumangala and M. S. Sreekanth. *J. Energy Storage*, 44 (2021) 10336.
3. Poonam, K. Sharma, A. Arora and S. K. Tripathi. *J. Energy Storage*, 21 (2019) 801.
4. K. V. G. Raghavendra, R. Vinoth, K. Zeb, C. V. V. M. Gopi, S. Sambasivam, M. R. Kummara, I. M. Obaidat and H. J. Kim. *J. Energy Storage*, 31 (2020) 801.
5. P. Simon and Y. Gogotsi. *Nat. Mater.*, 7 (2008) 845.
6. G. P. Wang, L. Zhang and J. J. Zhang. *Chem. Soc. Rev.*, 41 (2012) 797.
7. L. L. Zhang and X. S. Zhao. *Chem. Soc. Rev.*, 38 (2009) 2520.
8. Y. Zhang, H.-X. Mei, Y. Cao, X.-H. Yan, J. Yan, H.-L. Gao, H.-W. Luo, S.-W. Wang, X.-D. Jia, L. Kachalova, J. Yang, S.-C. Xue, C.-G. Zhou, L.-X. Wang and Y.-H. Gui. *Coord. Chem. Rev.*, 438 (2021) 213910.
9. L. Miao, Z. Song, D. Zhu, L. Li, L. Gan and M. Liu. *Energ. Fuel*, 35 (2021) 8443.
10. S. Yadav and A. Sharma. *J. Energy Storage*, 44 (2021) 103295.
11. V. Augustyn, P. Simon and B. Dunn. *Energ. Environ. Sci.*, 7 (2014) 1597.
12. W. T. Deng, X. B. Ji, Q. Y. Chen and C. E. Banks. *Rsc Adv.*, 1 (2011) 1171.
13. L. Feng, Y. Zhu, H. Ding and C. Ni. *J. Power Sources*, 267 (2014) 430.
14. R. S. Kate, S. A. Khalate and R. J. Deokate. *J. Alloys Compd.*, 734 (2018) 89.
15. C. D. Lokhande, D. P. Dubal and O. S. Joo. *Curr. Appl. Phys.*, 11 (2011) 255.
16. Y. Wang, J. Guo, T. Wang, J. Shao, D. Wang and Y.-W. Yang. *Nanomaterials*, 5 (2015) 1667.
17. Y. F. Zhang, L. Q. Li, H. Q. Su, W. Huang and X. C. Dong. *J. Mater. Chem. A*, 3 (2015) 43.
18. D. Chen, Q. Wang, R. Wang and G. Shen. *J. Mater. Chem. A*, 3 (2015) 10158.
19. L. Huang, D. Chen, Y. Ding, S. Feng, Z. L. Wang and M. Liu. *Nano Lett.*, 13 (2013) 3135.
20. J. Zhan, J. Chen and Y.-C. Wan. *J. Inorg. Mater.*, 34 (2019) 121.
21. L. Yu, G. Zhang, C. Yuan and X. W. Lou. *Chem. Commun.*, 49 (2013) 137.
22. C. Yuan, J. Li, L. Hou, X. Zhang, L. Shen and X. W. Lou. *Adv. Funct. Mater.*, 22 (2012) 4592.

23. G. Zhang and X. W. Lou. *Adv. Mater.*, 25 (2013) 976.
24. G. Q. Zhang, H. B. Wu, H. E. Hoster, M. B. Chan-Park and X. W. Lou. *Energ. Environ. Sci.*, 5 (2012) 9453.
25. M. M. Sk, C. Y. Yue, K. Ghosh and R. K. Jena. *J. Power Sources*, 308 (2016) 121.
26. C. Wang, E. Zhou, W. He, X. Deng, J. Huang, M. Ding, X. Wei, X. Liu and X. Xu. *Nanomaterials*, 7 (2017) 7020041.
27. S. Wang, S. Sun, S. Li, F. Gong, Y. Li, Q. Wu, P. Song, S. Fang and P. Wang. *Dalton Trans.*, 45 (2016)
28. T.-Y. Wei, C.-H. Chen, H.-C. Chien, S.-Y. Lu and C.-C. Hu. *Adv. Mater.*, 22 (2010) 347.
29. S. Wu, J. Liu, H. Wang and H. Yan. *Int. J. Energy Res.*, 43 (2019) 697.
30. Z. Wu, Y. Zhu and X. Ji. *J. Mater. Chem. A*, 2 (2014) 14759.
31. L. Shen, Q. Che, H. Li and X. Zhang. *Adv. Funct. Mater.*, 24 (2014) 2630.
32. L. Shen, L. Yu, X.-Y. Yu, X. Zhang and X. W. Lou. *Angew. Chem. Int. Ed.*, 54 (2015) 1868.
33. W.-W. Liu, C. Lu, K. Liang and B. K. Tay. *J. Mater. Chem. A*, 2 (2014) 5100.
34. Z. Luo, D. Shu, F. Yi, J. Ling, M. Wang, C. Huang and A. Gao. *New J. Chem.*, 45 (2021) 22748.
35. Y. P. Ma, X. B. Xie, W. Y. Yang, Z. P. Yu, X. Q. Sun, Y. P. Zhang, X. Y. Yang, H. Kimura, C. X. Hou, Z. H. Guo and W. Du. *Adv. Compos. Hybrid Mater.*, 4 (2021) 906.
36. Y. Li, X. Han, T. Yi, Y. He and X. Li. *J. Energy Chem.*, 31 (2019) 54.
37. J. Bao, X. Zhang, B. Fan, J. Zhang, M. Zhou, W. Yang, X. Hu, H. Wang, B. Pan and Y. Xie. *Angew. Chem. Int. Ed.*, 54 (2015) 7399.
38. S.-K. Chang, Z. Zainal, K.-B. Tan, N. A. Yusof, W. M. D. W. Yusoff and S. R. S. Prabaharan. *Ceram. Int.*, 41 (2015) 1.
39. H. Hu, B. Guan, B. Xia and X. W. Lou. *J. Am. Chem. Soc.*, 137 (2015) 5590.
40. W. Jiang, F. Hu, Q. Yan and X. Wu. *Inorg. Chem. Front.*, 4 (2017) 1642.
41. C. Jun, Z. Jing and W. a. N. Yu-Chi. *J. Inorg. Mater.*, 34 (2019) 121.
42. J. Li, L. Wang, Y. Yang, B. Wang, C. Duan, L. Zheng, R. Li, Y. Wei, J. Xu and Z. Yin. *Nanotechnology*, 32 (2021) 505710
43. J. Li, S. Xiong, Y. Liu, Z. Ju and Y. Qian. *Acs Appl. Mater. Inter.*, 5 (2013) 981.
44. X. Li, W. Sun, L. Wang, Y. Qi, T. Guo, X. Zhao and X. Yan. *Rsc Adv.*, 5 (2015) 7976